Computational Analysis of the Flow around a Surface Combatant at 10° Static Drift

Michel Visonneau, Emmanuel Guilmineau, Ginevra Rubino

▶ To cite this version:

Michel Visonneau, Emmanuel Guilmineau, Ginevra Rubino. Computational Analysis of the Flow around a Surface Combatant at 10° Static Drift. 7th HRLM, Symposium on Hybrid RANS-LES Methods, Sep 2018, Berlin, Germany. ⟨10.1007/978-3-030-27607-2_32⟩. ⟨hal-02571285⟩

HAL Id: hal-02571285

https://hal.science/hal-02571285v1

Submitted on 12 May 2020

Computational Analysis of the Flow around a Surface Combatant at 10° Static Drift

M. Visonneau[1] and E. Guilmineau[1] and G. Rubino[1]

CNRS/Centrale Nantes, 1 Rue de la Noë, Nantes, France,
`michel.visonneau@ec-nantes.fr`

Abstract. This paper presents a local and global computational study of the flow around the US Navy frigate DTMB 5415 at 10° static drift configuration. A thorough validation study comparing isotropic $k-\omega$ SST, non linear anisotropic EARSM statistical closures and the unsteady hybrid RANS-LES DES-SST model is conducted. This validation study includes detailed global and local comparisons with IIHR (Iowa Institute of Hydraulic Research) remarkable TPIV experiments. These validations are conducted on a very fine unstructured grid, which includes local boxes of refinement in the cores of the two main vortices, for a total number of 163M cells.

Keywords: static drift, validation study, hybrid RANS-LES

1 Introduction

The local flow around ships or submarines at straight ahead or static drift conditions is dominated by the onset and development of longitudinal vortices, which progress in the close vicinity of the hull. The accurate prediction of the right level of vorticity is crucial for the design of propellers and appendages, which operate in an averaged flow field heavily influenced by the presence of one or several interacting longitudinal vortices. In previous workshops on numerical ship hydrodynamics Gothenburg 2010 (G2010), see [2] and Tokyo 2015 (T2015) or research collaborative studies like NATO/AVT183, see [7], for IIHR experiments, it was demonstrated that the use of anisotropic turbulence models leads to a significantly better agreement with the measurements, as long as the averaged isowakes or longitudinal vorticity are concerned. However, the computations predicted levels of turbulent kinetic energy in the core of the averaged longitudinal vortices four to five times smaller than what is experimentally measured. The same failure was observed on very different ships (JBC and DTMB 5415) for various types of open separation (bilge or sonar dome vortices). This paper will present a complete validation study comparing isotropic $k-\omega$ SST, non linear anisotropic EARSM statistical closures, see [1], and an unsteady hybrid RANS-LES DES-SST model conducted for the static drift configuration, including a detailed local comparisons with IIHR TPIV experiments.

2 ISIS-CFD At A Glance

The solver ISIS-CFD, available as a part of the FINE^{TM}/Marine computing suite distributed by NUMECA Int., is an incompressible unsteady Reynolds-averaged Navier-Stokes (URANS) solver mainly devoted to marine hydrodynamics. The method features several sophisticated turbulence models, from the classical statical closures, isotropic and anisotropic, to Hybrid RANS-LES turbulence models based on Detached Eddy Simulation (DES-SST, IDDES). The solver is based on a generalized unstructured finite volume method to build the spatial discretization of the transport equations. Free-surface flow is simulated with a multi-phase flow approach: the water surface is captured with a conservation equation for the volume fraction of water, discretized with specific compressive discretization schemes, see [4].

3 IIHR EXPERIMENTS

The experiments used in this computational study were conducted in the towing tank facility at IIHR (all the details can be found in [7]). The hull form used in the tests was the DTMB 5512, a 1:46.6 scale, 3.048 m (L) long model, which is a geosim of the DTMB 5415, a 1:24.8 scale, 5.72 m model. The full-scale hull form is a preliminary design for a US Navy surface combatant. Characteristic features of the DTMB 5415 hull include a transom stern and a sonar dome bow. The ship model was tested in calm-water conditions at a $\texttt{Fr} = 0.28$, which corresponds to the full-scale cruise speed of 20 knots and to a model scale towing speed of 1.53 m/s. The model scale Reynolds number $\text{Re} = 4.65 \times 10^6$ is based on a nominal water temperature of 20°C. The data to which we are going to refer in the present context include: forces and moments, longitudinal variations of flow variables in the core of the vortex, contours of flow variables at several planes along the hull. The flow topology was accurately described in [7] and one will retain the definition of the main vortices proposed in this publication. Taken from IIHR studies, Fig. 1 shows an overview of the vortical structures in experiments and computations.
In the Figure 1, one can distinguish three major co-rotating structures:

- **SDTV**, Sonar Dome Tip Vortex. It originates from the sonar dome end tip and it progresses along the hull in a straight line fashion.
- **BKTV**, Bilge Keel Tip Vortex. It originates from the windward bilge keel surface. Its intensity is comparable with the SDTV.
- **ABKV**, Aft Body Keel vortex. It appears in correspondence of the section $X/L = 0.8$. The vortex initially proceeds downstream following the windward side, then it deflects across the hull centerline and it appears on the leeward side of the hull.

From Fig. 1, other minor structures are visible: the LW-SDV (LeeWard Sonar Dome Vortex), the WW-FBKV and the LW-FBKV (WindWard and LeeWard Fore Body Keel Vortex) and the BKV (Bilge Keel Vortex). In this study, our attention will be focused on the analysis of the numerical results relative to the two main vortices: the so-called SDTV and BKTV vortices.

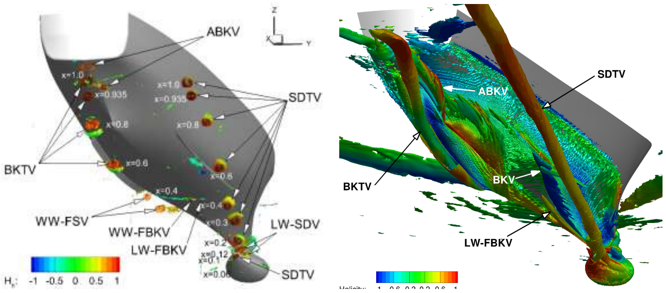

(a) TPIV measurement. (b) ISIS-CFD computation.

Fig. 1: Iso-Q surfaces ($Q = 50$) colored by the normalized helicity level by TPIV measurements and by ISIS-CFD using hybrid RANS-LES

4 VALIDATION STUDY

In a previous study, a first comprehensive verification and validation study was carried out, paving the way to this article. A grid sensitivity study led to recommendations which are by far exceeded to build the very fine grid of 163 million cells (for additional details, see [5]). In order to compare the linear isotropic $k-\omega$ SST and non-linear anisotropic EARSM statistical turbulence closures with the DES-SST unsteady hybrid RANS-LES model, three computations on the 163M grid are compared from a global and local viewpoints.

4.1 Numerical settings

The computational domain starts $1.5L$ in front of the model and extends up to $2.5L$ behind the hull. The width of the computational domain is $4L$ and the height is 2L with $1.5L$ below the free surface at rest. The mesh is generated by Hexpress$^{\text{TM}}$, an automatic unstructured mesh generator. This software generates meshes containing only hexahedrons. Three refinement boxes are used: one including the hull with a cell size of 10 mm in each direction; a second including the sonar dome and extending until $X/L = 1.0$; a third box which starts at the beginning of the windward bilge keel and extends until $X/L = 1.0$. For these two latter boxes, the cell size is Δx = 1.5 mm and Δy = Δz = 0.7 mm. Finally, a last box, generated through the use of ISIS-CFD adaptive grid refinement, is used and covers the sonar dome. In this box, all cells are twice smaller. All the boxes are aligned with the main flow direction. The final mesh contains 162.6 million cells. On this grid, the averaged value of $y^+ = \frac{u_\tau y}{\nu}$ is 0.129, resulting in a first layer dimensionless thickness of the order of 7×10^{-6}. Two RANS turbulence models are used: $k-\omega$ SST and a non linear anisotropic EARSM, based on the $k-\omega$ model. A hybrid RANS-LES turbulence model based on DES is also employed. With the DES model, the F_{DES} function allows the switch between RANS mode (F_{DES} = 1) and LES mode ($F_{DES} > 1$). On our grid, the RANS area covers approximately 20 cells in the normal direction to the hull. With the DES model, the F_{DES} function allows the switch between RANS mode (F_{DES} = 1) and LES mode ($F_{DES} > 1$). On our grid, the RANS area covers approximately 20 cells in the normal direction to the hull. For the RANS simulations, the time step is Δt = 2×10^{-2} s, while for the DES, the time step is Δt = 5×10^{-4} s and the non-dimensional averaging time, $t \times U/L$, is 5.2.

4.2 Forces

Table 1 shows the longitudinal, lateral forces and yaw moment for each computations. The agreement with the IIHR experiments on the longitudinal force is very good for both statistical turbulence closures, however the non-linear anisotropic model improves significantly the prediction of the lateral force. On the other hand, the hybrid RANS-LES computations are far less satisfactory. Comparisons between viscous and pressure resistances of the different turbulence models indicate that both components are significantly under-estimated by DES-SST. This error on the viscous resistance should probably be attributed to the problem of log-layer mismatch reported in [3]. Predictions could be improved by using a better shielding function to protect the boundary layer from the influence of the so-called gray zone.

4.3 Global time-averaged flow field

Figs 2a and 2b provide a global windward view of the main time-averaged vortical structures created around the DTMB 5415 at 10° static drift. These figures show the main longitudinal vortices, as computed on the same grid by the $k-\omega$ SST and the hybrid RANS-LES models. The time-averaged vortical structures do not differ much in terms of location and longitudinal extent between the two

Table 1: DTMB at 10° static drift - Forces and moment coefficients

Coeff. [*10^3]	IIHR exps.	$k-\omega$ SST	EARSM	DES-SST
C_x	-19.61	-19.41 (-1.03%)	-19.35(-1.33%)	-16.37 (-16.54%)
C_{xp}		-6.85	-6.75	-5.36
C_{xv}		-12.56	-12.60	-11.01
C_y	58.46	55.63 (-4.84%)	58.18 (-0.47%)	63.96 (9.41%)
C_N	28.61	29.35 (2.60%)	29.28 (2.35%)	29.41 (2.80%)

turbulence models. However, one can notice that DES-SST provides an SDTV vortex with a radius which is smaller all along its progression compared to its RANS-based counterparts, indicating a more intense longitudinal vorticity. The next figures present two detailed views of the onset of the vortices at the sonar dome at the windward and leeward sides. Fig. 3a and Fig. 3b show the onset of the SDTV vortex on the windward side. SDTV detaches from the tip of the windward side of the sonar dome, slightly before the vertical trailing edge. Once SDTV enters the near wake of the trailing edge, the separation along the keel line takes place with a visible layer of detachment starting from the vertical plane of symmetry. The SDTV vortex progresses up to the stern of the ship without being noticeably damped due to the presence of a very fine local parallelipedic box of refinement located in its core. Such a topology on the windward side of the sonar dome is observed with every tested turbulence closures. In Fig. 3c and Fig. 3d, showing the leeward side, the situation appears a bit more complex. First of all, one can notice a small closed zone of recirculation located between the free-surface and the intersection between the stem of the ship and the sonar dome, characterized by a small helicity. While progressing downwards from the free-surface to the sonar dome, one can notice a first wing-body junction like vortex with a positive helicity. This vortex progresses in the junction between the hull and the sonar dome and joins SDTV. This wing-body junction vortex is accompanied by a counter-rotating longitudinal vortex which seems to detach from the upper part of the sonar dome, progresses along the hull and vanishes quickly, probably mitigated by the local numerical dissipation. This vortex was identified in [7] as Leeward Sonar Dome Vortex (LW-SDV). A third longitudinal vortex with a positive helicity emerges from the middle part of the sonar dome. It looks like a tip vortex, but is very quickly attracted by the main SDTV vortex which emerges from the windward side behind the sonar dome trailing edge. It is reassuring to notice that the same number of vortices and locations of onset is observed for statistical and hybrid RANS-LES closures. However, the LW-

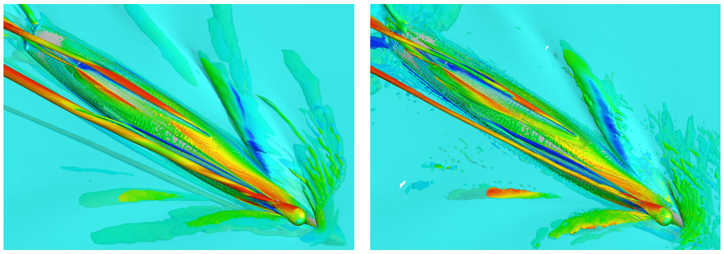

(a) $k-\omega$ SST (b) DES SST

Fig. 2: Global views of the time-averaged $Q^* = 50$ surfaces colored by the helicity on the windward side of the DTMB 5415 for $k-\omega$ SST and DES SST turbulence models

SDV and SDTV vortices predicted by DES-SST appear to be more intense, as indicated by the smaller radius of their respective iso Q^* surfaces.

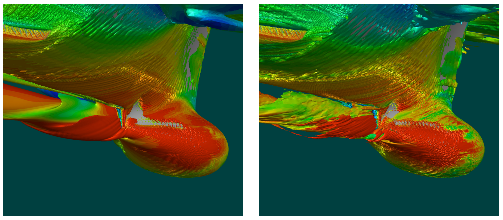

(a) $k-\omega$ SST (b) DES-SST

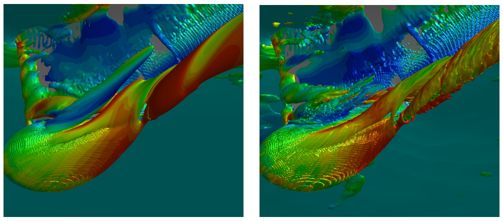

(c) $k-\omega$ SST (d) DES-SST

Fig. 3: Time-averaged $Q* = 50$ structures on the leeward side of the sonar dome for various turbulence closures

4.4 Cross-sections

IIHR performed several measurements of the velocity fields, longitudinal vorticity and turbulence kinetic energy at several cross-sections. The results at the various sections, as computed by the different turbulence models, are discussed in details in [6]. Therefore, since the scope of this paper is to highlight the striking differences between the various closures, only the turbulence kinetic energy contours at two enlightening sections will be shown. Firstly, at the section $X/L = 0.300$ of the hull, shown in Fig. 4, the main SDTV vortex starts to leave the vicinity of the hull. One can notice that while both statistical turbulence closures predict a very low level of tke in the core of the vortex, trend reinforced by the non-linear anisotropic model, the hybrid RANS-LES is the only one which captures a level of tke in the core of the SDTV vortex at this location in accordance with the experimental results. Indeed, the relaminarization of the core of the vortex during its progression predicted by the statistical closures is not confirmed by the IIHR experiments. Then, Fig. 5 shows the cross-sectional distribution of tke at section $X/L = 0.600$, further away from the hull. The observations reported previously are fully confirmed here. IIHR experiments reveal without any ambiguity that the high level of tke is still present and sustained in the core of the SDTV vortex. Moreover, the same characteristic is observed in the core of the BKTV vortex since a red spot of tke is also clearly visible. This high level of tke in the core of all the observed longitudinal vortices is only reproduced by the hybrid RANS-LES closure. In addition, even the onset of the BKTV vortex appears satisfactorily captured despite the modeling uncertainties linked to the influence of the so-called gray region. Indeed, this vortical structure rises inside the boundary layer, next to the location where the model switches from RANS to LES. Up to the stern of the ship, experiments and, uniquely, hybrid RANS-LES computations show that the cores of the SDTV and BKTV vortices remain highly turbulent with no trend towards a relaminarization, revealing a main difference between the various closures.

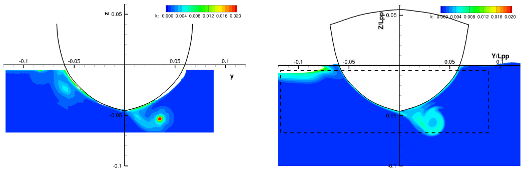

(a) Experiments (b) $k-\omega$ SST

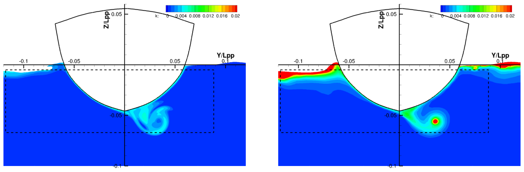

(c) EARSM (d) DES-SST

Fig. 4: Turbulence kinetic energy at $X/L = 0.300$

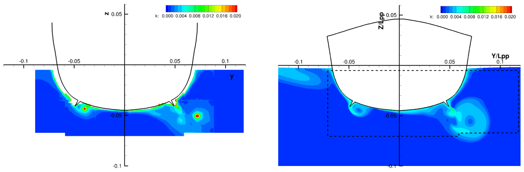

(a) Experiments (b) $k-\omega$ SST

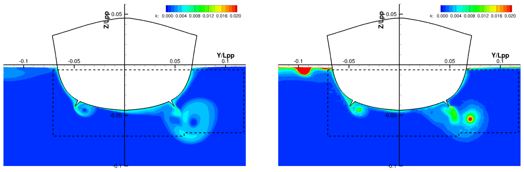

(c) EARSM (d) DES-SST

Fig. 5: Turbulence kinetic energy at $X/L = 0.600$

4.5 Longitudinal evolution

Based on their accurate TPIV measurements at several X/L sections, IIHR was able to locate experimentally the centers of SDTV and BKTV vortices by determining the maximum value of the second invariant Q. They measured at these locations various quantities as the turbulence kinetic energy k. Fig. 6 provides a comparison between the IIHR measurements and the present computations. Large differences between the turbulence modeling approaches can be observed on the prediction of the second invariant Q. DES-SST provides a value of Q in far better agreement with the measurements than the $k-\omega$ SST model, which is unable to avoid the progressive damping of the SDTV vortex during its progression. At some sections (e.g. $X/L = 0.600$ or $X/L = 0.800$), the value of Q predicted by DES-SST is almost ten times stronger than the one predicted by $k-\omega$ SST. One notices also that DES-SST appears to be less accurate on the prediction of BKTV. This might be related to the fact that the onset of BKTV is located in the gray region of the hybrid RANS-LES closure. The most remarkable difference between the statistical and hybrid RANS/LES turbulence models is provided by the comparison on the longitudinal evolution of the turbulence kinetic energy in the core of the vortices. DES-SST is clearly the only model able to predict the right level of turbulence kinetic energy in the core of SDTV and BKTV. $k-\omega$ SST and EARSM strongly underestimate by one to two orders of magnitude the turbulence kinetic energy in the core of SDTV, for instance. Thus, the real physics of the flow is not correctly represented by these statistical turbulence closures, even if anisotropy is partially accounted for in EARSM.

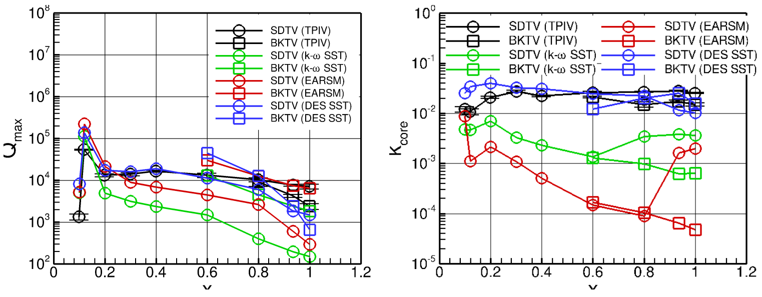

(a) Q (b) TKE

Fig. 6: Longitudinal evolution of the second invariant Q and turbulence kinetic energy k along the core of SDTV and BKTV vortices

4.6 Onset of Separation

In order to better understand the mechanisms controlling the onset of separation at the sonar dome, it is necessary to come back to the unsteady flow which provides us with the true flow physics. Fig. 7 shows the instantaneous vortical structures at the leeward and windward sides, as computed by the hybrid RANS-LES model. On the leeward side, a population of ring vortices are created between the free-surface and the top of the sonar dome, indicating that the time averaged closed separation and wing-body junction like vortices mentioned in the section 4.3 are actually characterized by very intense velocity fluctuations. This unsteadiness is reflected by the periodic shedding of ring vortices of various helicities which are deformed and convected along the hull in the vicinity of the top of the sonar dome and, finally, they enter the core of the SDTV vortex. This unsteady region of separation contributes to feed the core of SDTV with ring-like vortices of negative helicities. On the other hand, the same figure shows, just after the onset of the LW-SDV vortex, a quick destabilization characterized by a succession of ring-like vortices of weak positive helicities. Finally, viewed from the leeward side, the SDTV vortex appears also composed of a succession of intense ring-like vortices of strong positive helicities. As illustrated by Fig. 8, the core of the SDTV vortex appears to be composed of a multitude of unsteady ring-like vortices of various helicities. They come both from the periodic shedding at the trailing edge of the sonar dome and from the unsteady separation present on the leeward side which sheds vortical structures later attracted in the core of SDTV. All these unsteady large scale vortices of various helicities are entrained in a global rotation motion around the unsteady axis of SDTV, creating a high level of resolved velocity fluctuations in its core. This provides a convincing explanation of the high level of turbulence kinetic energy observed in the measurements all along the progression of the vortex.

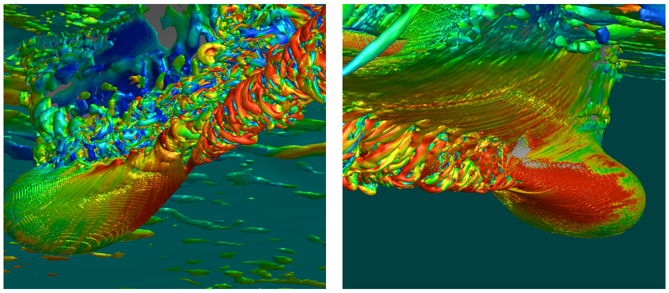

(a) Instantaneous (b) Instantaneous

Fig. 7: DES-SST - Instantaneous $Q^* = 50$ structures on the leeward (left) and windward (right) sides of the sonar dome

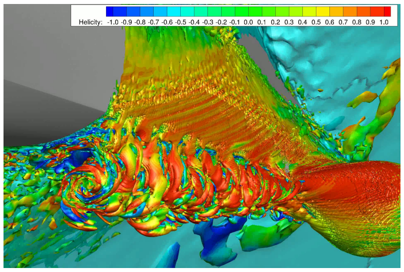

Fig. 8: DES-SST - Cross-sectional view of the instantaneous SDTV vortex, visualized through the iso-surface $Q^* = 50$, at $X/L = 0.300$

5 Conclusion

The detailed analysis of the 10° static drift flow condition leads to several important results. The origin of the high level of turbulence kinetic energy,detected by the experiments in the core of the SDTV vortex, has been accurately captured by the unsteady DES-SST closure. None of the tested statistical turbulence models was able to catch this flow physics, because it is essentially unsteady and linked with vortex shedding on the leeward side and on the trailing edge of the sonar dome. The additional turbulence anisotropy of the Reynolds stress algebraic formulation seems to increase the local vorticity in the core of the vortex, but at the expense of a degradation of the predicted turbulence kinetic energy. The unsteady RANS-LES model is the only approach able to represent the true flow physics, which shows a co-existence of a high level of turbulence kinetic energy in the core of the vortex and a high level of vorticity, which is not attenuated by turbulent diffusion during the progression of the vortex to the end of the ship.

Acknowledgements

The computations were performed using HPC resources from GENCI (Grand Equipment National de Calcul Intensif)(Grant2016-2a0209, Grant2017-2a0129), which is gratefully acknowledged. The help of Dr. Hyunse Yoon and Professor Frederick Stern from IIHR, who provided us with these remarkable experiments at an early stage of this work, is warmly acknowledged.

References

1. Deng, G., Visonneau, M.: Comparison of explicit algebraic stress models and second-order turbulence closures for steady flows around ships. Proc. 7th Int. Conf. on Numerical Ship Hydrodynamics, Nantes, France (1999)
2. Larsson, L., Stern, F., Visonneau, M.: Numerical ship hydrodynamics, an assessment of the Gothenburg 2010 workshop, Springer Verlag (2013)
3. Nikitin, N.V., Nicoud, F., Wasistho, B., Squires, K.D., Spalart, P.R., An approach to wall modelling in Large-Eddy simulations. Phys.Fluids Vol. 12, 1481-1510 (2007)

4. Queutey, P., Visonneau, M.: An interface capturing method for free-surface hydrodynamic flows. Computers & Fluids Vol.36, 1481-1510 (2007)
5. Rubino, G.: Large dynamic manoeuvers for a naval vehicle. Master Research Thesis, Centrale Nantes (2017)
6. Visonneau, M., Guilmineau, E., Rubino, G.: Computational analysis of the flow around a surface combatant at 10° static drift and dynamic sway conditions. 32nd Symposium on Naval Hydrodynamics, Hamburg, Germany (2018)
7. Yoon, H., Gui, L., Bhushan, S., Stern, F.: Tomographic PIV measurements for a surface combatant at straight ahead and static drift conditions. 30th Symposium on Naval Hydrodynamics, Hobart, Australia (2014)